ACS SENSORS

Article

Cite This: ACS Sens. 2018, 3, 1499−1509

pubs.acs.org/acssensors

Nanoplasmonics for Real-Time and Label-Free Monitoring of Microbial Biofilm Formation

Riccardo Funari,*[,†,¶] Nikhil Bhalla,[†,¶] Kang-Yu Chu,[†] Bill Söderström,[‡] and Amy Q. Shen*[,†]

[†]Micro/Bio/Nanofluidics Unit and [‡]Structural Cellular Biology Unit, Okinawa Institute of Science and Technology Graduate University, 1919-1 Tancha, Onna-son, Okinawa 904-0495, Japan

Supporting Information

ABSTRACT: Microbial biofilms possess intrinsic resistance against conventional antibiotics and cleaning procedures; thus, a better understanding of their complex biological structures is crucial in both medical and industrial applications. Existing laboratory methodologies have focused on macroscopic and mostly indirect characterization of mechanical and microbiological properties of biofilms adhered on a given substrate. However, the kinetics underlying the biofilm formation is not well understood, while such information is critical to understanding how drugs and chemicals influence the biofilm formation. Herein, we report the use of localized surface plasmon resonance (LSPR) for real-time, label-free monitoring of *E. coli* biofilm assembly on a nanoplasmonic substrate consisting of gold mushroom-like structures. Our LSPR sensor is able to capture the signatures of biofilm formation in real-time by measuring the wavelength shift in the LSPR resonance peak with high temporal resolution. We employ this sensor feature to elucidate how biofilm formation is affected by different drugs, including conventional antibiotics (kanamycin and ampicillin) as well as rifapentine, a molecule preventing cell adhesion yet barely affecting bacterial viability and vitality. Due to its flexibility and simplicity, our LSPR based platform can be used on a wide variety of clinically relevant bacteria, thus representing a valuable tool in biofilm characterization and drug screening.

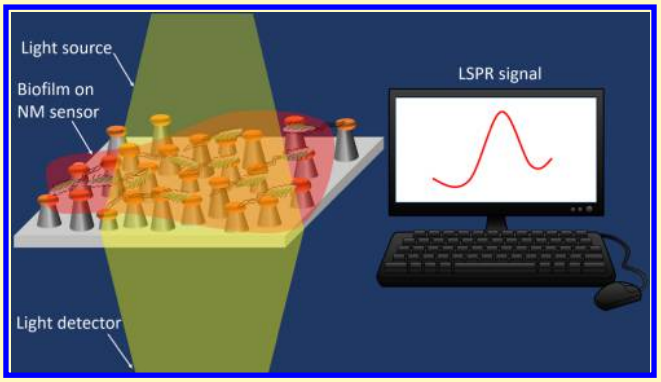

KEYWORDS: *biofilms, real-time monitoring, LSPR, antibiotics, drug screening, E. coli*

Bacteria exhibit two types of growth regimes: planktonic, where cells are freely moving in a bulk solution, and sessile aggregates known as biofilms.[1,2] In the latter form, the microorganisms are closely packed on a solid surface within self-produced matrix of extracellular polymeric substances (EPS). This structure provides many structural and functional benefits such as improved resource capture, adhesion to surfaces, digestive capacity, protection against external agents, and inhibition of bacterial dehydration. Furthermore, the EPS scaffold facilitates intercellular interactions and horizontal gene transfer.[3] Another key feature of bacterial biofilms concerns the development of their peculiar resistance against antimicrobial agents.[4] Some of their possible protection strategies involve poor antibiotic penetration, formation of gradients of nutrients or cell products, and phenotypic differentiation induced by the EPS matrix.[5,6] In addition, the lack of nutrients and the high concentrations of bacterial metabolites in biofilms result in areas where cells are in a stationary phase (a slow or nongrowth phase of bacterial growth cycle), which become mostly immune to conventional antibiotic drugs since they target specifically to the metabolically active microorganisms.[7]

Because of their unique properties, bacterial biofilms have been actively studied across diverse fields, ranging from industrial processes to medicine. For example, biofilms have been used in bioremediation, waste treatment, and production of fine chemicals and biofuels.[8] On the other hand, biofilms are associated with serious health issues stemming from persistent infections due to the contamination of medical devices (e.g., intravenous and urinary catheters), artificial implants,[9] and pollution of drinking water.[10] Similar concerns have been recently raised by the world health organization (WHO) through their first global antimicrobial resistance surveillance system (GLASS) report.[11] In this context, bacterial detection, antibiotic susceptibility, and the rise of antibiotic resistant microorganisms are pressing issues requiring novel and sensitive detection strategies which can also be adopted to screen new drugs. For instance, Jo et al.[12] recently developed a capacitive aptamer-based biosensor to monitor the bacterial growth and antibiotic susceptibility in real-time. In another study, Brosel-Oliu et al.[13] detected pathogenic *E. coli* using impedance spectroscopy. However, both approaches focused on the detection of single planktonic bacteria instead of microbial biofilm formation. In contrast, biofilm assembly requires the direct adhesion of the bacterial cells onto the

Received: April 9, 2018
Accepted: July 31, 2018
Published: July 31, 2018

DOI: 10.1021/acssensors.8b00287
ACS Sens. 2018, 3, 1499−1509

Table 1. Overview of the Latest Techniques for Bacterial Biofilm Characterization

method	real-time kinetics: temporal resolution	cost of system	assay type	throughput	drug screening	limitations	key references
Biofilm Ring Test	Yes ≲1 h	Low	Labeled	Low	No		14
Microtiter plates	No N/A	Low	Labeled	High	Yes		15,16
Staining Assays (e.g., Crystal Violet)	No N/A	Low	Labeled	Low	Yes	All these techniques are laboratory based, unsuitable for on-site testing of bacterial biofilms and require user to have highly specific technical skills to perform measurements	17
Drop Flow Reactors	Yes N/A	High	Labeled	Low	No		18
Rheometers	Yes Tunable (max 1 s)	High	Label-free	Low	No	Only suitable to study mechanical properties of biofilm	19
Atomic Force Microscopy	No Tunable (max 0.1 s)	High	Label-free	Low	No	Even though AFM can provide detailed information on the adhesive and structural properties of biofilm, the complexity of the imaging procedure strongly limits the use of this methodology for high throughput tests.	20−23
Quartz Crystal Microbalance	Yes Tunable (max 0.1 s)	Low	Label-free	Low	Yes	Cross sensitivity against density and viscoelastic properties in the bulk media	24
Electrochemical Impedance Spectroscopy	Yes ≲30 s per scan	High	Label-free	Low	Yes	Cross sensitivity to mass and charge transport of analyte which affects sensor stability	13,25−27
Capacitive sensors based on aptamers	Yes ≲3 min per scan	High	Labeled	High	Yes	The use of aptamers for catching specific bacteria prevents studying bacterial biofilms in native conditions	12
Field Effect Sensors	Yes Tunable (max 0.1 s)	Low	Label-free	Low	Yes	Unstable measurements due to electrical noise and material biocompatibility issues at nanoscale	28
Surface Plasmon Resonance	Yes Tunable (max 1 s)	High	Label-free	Low	Yes	Prone to changes in bulk solution and hence large noisy in turbid media	29
PCR	Yes ≲1 min	High	Labeled	High	Yes	Cross sensitivity and selectivity issues with nonspecific DNA	30
FTIR spectroscopy	Yes ≲5 s	High	Label-free	Low	No	Requires time-consuming post measurement analysis to identify peaks related to signatures of biofilm formation	31
Microfluidics	Yes ≲1 s	High	Labeled/ Label-free	High	Yes	Small volumes make it difficult to analyze turbid samples. Microfluidics often require integration of sensors or microscopy tools to validate biofilms.	32
Localized Surface Plasmon Resonance	**Yes** **Tunable (max 1 s)**	**Low (≲200 USD)**	**Label-free**	**High**	**Yes**	**Sensitivity/biocompatibility trade off**	**This work**

DOI: 10.1021/acssensors.8b00287
ACS Sens. 2018, 3, 1499−1509

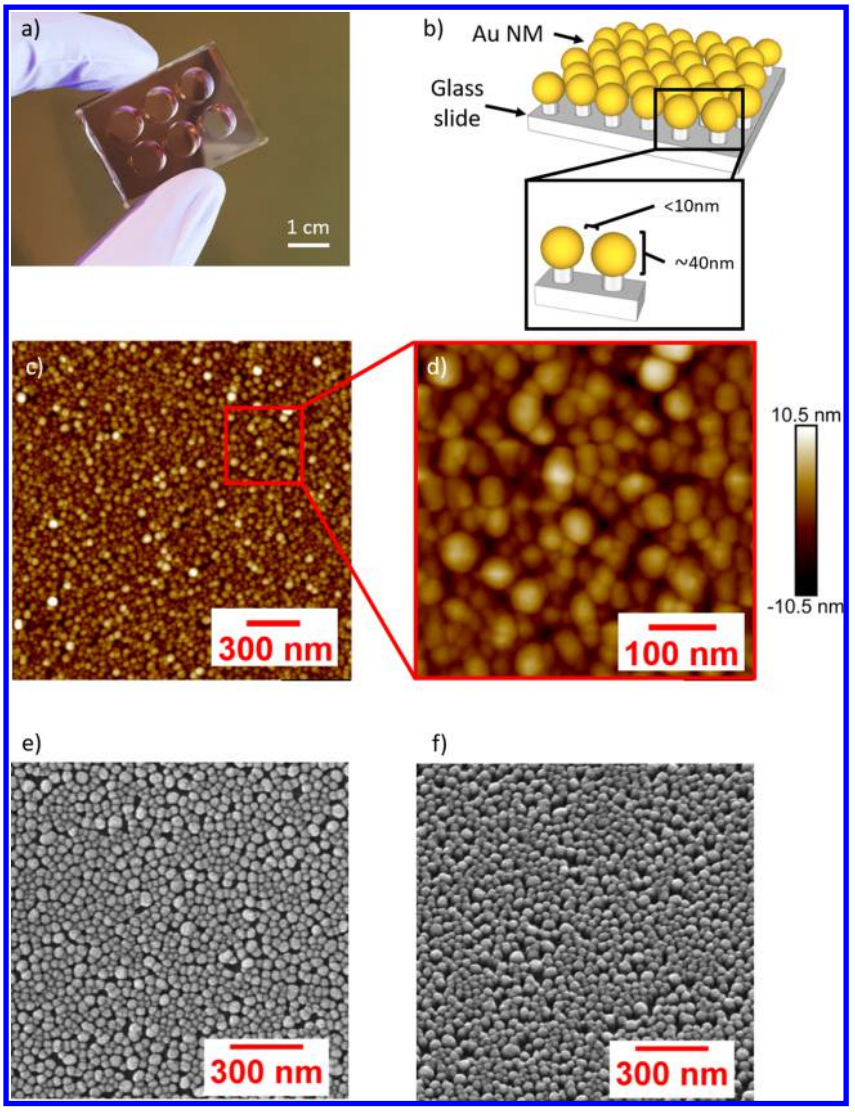

Figure 1. LSPR biochip and microscopic characterization of the plasmonic nanostructures. (a) Snapshot of the device. (b) Schematic of the Au NM LSPR substrate. In order to monitor the bacterial biofilm formation, the nanostructured glass substrate bonds with a PDMS slab containing multiwell structures, where each well can accommodate up to 150 μL of cell suspensions. The AFM scan of the Au NM substrate with (c) a 2 μm × 2 μm scan area; (d) magnification of a 500 nm × 500 nm area. This set of measurements shows the uniformity of the Au NM, with an average roughness of 2.0 ± 0.1 nm. SEM images of Au NMs acquired at 100 000× magnification: (e) top; and (f) tilted (40°) images.

substrate because the use of a capturing element (e.g., aptamers or antibodies) prevents the biofilm detection under its native condition. Moreover, since bacteria in biofilms are extremely resistant to conventional drugs, there is a tremendous interest in discovering new biofilm specific antibiotics that can penetrate the polymeric matrix, thus reaching bacterial cells, and/or affecting the EPS structure to destabilize the biofilm so that standard antibiotics can subsequently attack the microorganisms.

Motivations described above underpin the research on developing reliable characterization tools to provide the real-time monitoring of biofilm formation under different drugs and chemicals. This activity is promising since detailed information on the biofilm growth kinetics is extremely valuable in discovering novel treatments and drugs to combat biofilm related infections (e.g., types and concentrations of antibiotics to use). A comparative overview of the latest technologies reported for the characterization of bacterial biofilm is summarized in Table 1 while more details about these methodologies can be found in the Supporting Information.

Recently, nanomaterial based label-free photonic biosensors have revealed unprecedented information on DNA and protein molecular interactions, finding wide applications in medical diagnostics, food safety, and environmental monitoring.[33,34] However, few attempts have been made to apply label-free photonic biosensors to cellular assays, as it is challenging to develop nanostructured substrates with large surface areas that promote both sensing and long-term cell survival. Localized surface plasmon resonance (LSPR) is the coherent oscillation of the surface electrons of metal nanostructures due to interactions between the incident light and the conduction band electrons of the metal.[35,36] This technology has been utilized to perform highly sensitive label-free detection of biomolecular interactions in real time, an essential feature for the early detection of diseases and point-of-care (POC) clinical evaluations. However, most recent uses of plasmonic materials

DOI: 10.1021/acssensors.8b00287
ACS Sens. 2018, 3, 1499−1509

on biofilms exploited the local temperature increase induced by the LSPR effect to prevent biofilm formation.[37−39]

We have recently demonstrated a biocompatible nanoplasmonic substrate by developing a gold-based nanoplasmonic material for long-term monitoring of eukaryotic cell proliferation.[40] In this work, by using a similar nanofabrication protocol, we report the use of LSPR for characterizing biofilm formation on a highly sensitive, large-scale, and biocompatible nanoplasmonic substrate containing high density gold nanomushroom structures. Our LSPR substrates consist of gold mushroom-like structures, with stems of silicon dioxide and caps of gold on the order of 30 nm in diameter, to achieve the LSPR effect. Specifically, the model organism *Escherichia coli* (*E. coli*) is used for all studies. The localized surface plasmons on the nanomushroom caps are exploited to monitor biofilm formation without any labeling procedure. In addition, we have developed an automated high resolution system allowing the real-time monitoring of biofilm formation by continuously illuminating the LSPR biochip in a Faraday cage and recording the resonance peak shift every minute for 24 h. Since LSPR effect is very sensitive to changes of a few tens of nanometers from the sensor surface, our methodology enables precise monitoring of the activities in the bottom layer of the adhering biofilm, which is difficult to achieve by using conventional techniques. This information is of paramount importance for fighting persistent infections in biofilms, since the microbial cells in direct contact with the substrate are mostly protected from the external environment, thus guarded against antibiotic treatment. As a proof of concept study, we further apply our LSPR chips to investigate how three different types of antibiotics affect the *E. coli* growth as well as the biofilm formation. We demonstrate that our biochip serves as a powerful characterization tool for investigating real-time biofilm formation, screening of new drugs, and evaluating alternative cleaning procedures.

EXPERIMENTAL SECTION

Bacterial Growth. Precultures of wild type strain MC4100 (K12 derivative) are grown overnight in a 20 mL lysogeny broth (LB) (rich media), shaken at 200 rpm at 37 °C. The cultures are back-diluted to 1:200 in a fresh LB media after overnight culture. This roughly corresponds to 2×10^7 CFU mL^{-1}, as estimated from counting single colonies from serial dilutions on LB-agarose filled Petri dishes. The cultures are gently vortexed before a volume of 125 μL of the sample is directly aliquoted into the microwells of the LSPR biochip.

LSPR Biochip Fabrication. The gold (Au) nanomushroom (NM) based LSPR chip is fabricated by a 3-step process. First, we deposit 5 nm Au film onto a SiO_2 substrate at 0.1−0.2 Å s^{-1} using an e-beam evaporator (KE604TT1-TKF1, Kawasaki Science) in a class 1000 clean room. Prior to deposition, SiO_2 substrates were cleaned with acetone and isopropanol. Next we anneal the 5 nm gold film at 560 °C for 3 h to generate a distribution of Au nanoislands on the SiO_2 substrate. Finally, we selectively etch the Au nanoislands on SiO_2 to generate mushroom like structures using reactive ions of SF_6. The reactive ion etching (RIE) is performed by inductively coupled plasma (ICP) chemical vapor deposition equipment (Plasmalab 100, Oxford Instruments). SF_6 gas is introduced inside the RIE-ICP chamber, maintained at an inside pressure of 10 mTorr and a flow rate of 45 sccm (standard cubic centimeters per minute). The RF power coil and the RF bias coils are fixed to 150 and 10 W, respectively, and the temperature inside the plasma chamber is maintained at 5 °C. The total duration of RIE is 5 min. More details on the fabrication techniques can be found in our recent work.[41]

To fabricate PDMS wells, we first make slabs of PDMS by pouring 10:1 polydimethylsiloxane (PDMS) (Dow Corning, Japan) in a Petri dish and then cure the prepolymer for 3.5 h at 60 °C after degassing to remove air bubbles. We then punch holes of 8 mm in diameter by using disposable biopsy punchers (Kai Medical, Japan) to create PDMS wells. Both PDMS and the NM substrate are exposed to oxygen plasma (Harrick Plasma, USA) at 30 W for 1 min. After plasma treatment, PDMS well and NM based LSPR substrate are immediately brought in close contact to ensure strong bonding (Figure 1a). This treatment ensures proper confinement of the sample solution without any leakage. Thereafter the developed LSPR biochips are used for bacterial biofilm sensing.

Morphological Characterization of the LSPR Substrate. AFM imaging is performed in tapping mode using a Dimension Icon3 (Bruker, Japan) microscope equipped with an aluminum back-coated, antimony-doped Si cantilever from Bruker (TESPA-V2), with typical values of a nominal tip radius ∼8 nm, spring constant $k \approx 42$ N m^{-1}, and resonance frequency $f_0 \approx 320$ kHz. Areas of 4 μm^2 and 0.25 μm^2 have been scanned under a scanning speed of 1 Hz, with a resolution of 512 pixels per line, and a relatively high amplitude set-point ratio ($A_{sp}/A_{free} \approx 0.85$; $A_{free} \approx 23$ nm; $A_{sp} \approx 17$ nm). All the measurements have been repeated three times and the experimental results have been processed using NanoScope Analysis 1.8 software (Bruker, USA).

The scanning electron microscopy (SEM) is carried out by using a high performance scanning electron microscope (FEI Quanta 250 FEG, Thermo Fisher Scientific). Images are acquired at 20 kV, with a magnification of 100 000× inside a vacuum chamber maintained at a pressure of 10^{-4} Pa. To avoid charging of SiO_2 surfaces during imaging, the NM substrates are coated with Pt/Pd at a few angstroms thickness. The top view of the NM substrate is captured with the electron gun placed normal to the substrate. In contrast, the side view of the NM substrate is captured by tilting the electron gun at 40°. The SEM images are processed with ImageJ software to analyze detailed morphological features such as the size and gaps between the NM structures.

Sensing Procedure. The instrument involving LSPR consists of two fiber optics patch cords, one connected with a halogen light source (LS-1-LL) and the other connected to the spectroscope (USB4000-UV-vis-ES). All discrete components (spectrometer, light source, and patch chords) are purchased from Ocean Optics (Japan). The LSPR signals are acquired in T-LSPR (Transmission) mode. Before taking any signal from the spectroscope, the system is calibrated for dark and light spectrum modes. The LSPR signal is then recorded in absorption mode by observing the wavelength dependence of the light absorbed by Au NM via the Spectrasuite software (cross-platform spectroscopy operating software from Ocean Optics). For noncontinuous experiments, the biochip containing the bacteria grows in a Taitec BR-23PF incubator (Japan) under 37 °C, but the biochip is removed from the incubator periodically for the absorption spectrum acquisition under room temperature. The real-time measurements are performed in a Faraday cage under continuous illumination for 24 h. The real-time measurements are acquired by processing the spectrometer data through a homemade graphics user interface on a Matlab platform. The data are then analyzed using OriginPro 2017 (OriginLab, USA).

Crystal Violet Staining. Crystal violet (CV) assay is a well established methodology to evaluate biofilm formation under various growth conditions (e.g., drug screening, strain comparison).[42,43] For this reason, the CV assay is used to validate the measurements from our LSPR biochip system. The detailed procedure is reported in the Supporting Information.

Viability Staining. LIVE/DEAD BacLight Bacterial Viability Kit (L13152) from Invitrogen has been used to evaluate cell viability on Au NM LSPR substrate and investigate the effect of the continuous white light illumination on *E. coli* cells. The detailed protocol is reported in the Supporting Information.

RESULTS AND DISCUSSION

Characterization of the Nanoplasmonic Chip. An integrated LSPR biochip (Au NM LSPR substrate bonded with PDMS wells) is shown in Figure 1a. The nanostructured

DOI: 10.1021/acssensors.8b00287
ACS Sens. 2018, 3, 1499−1509

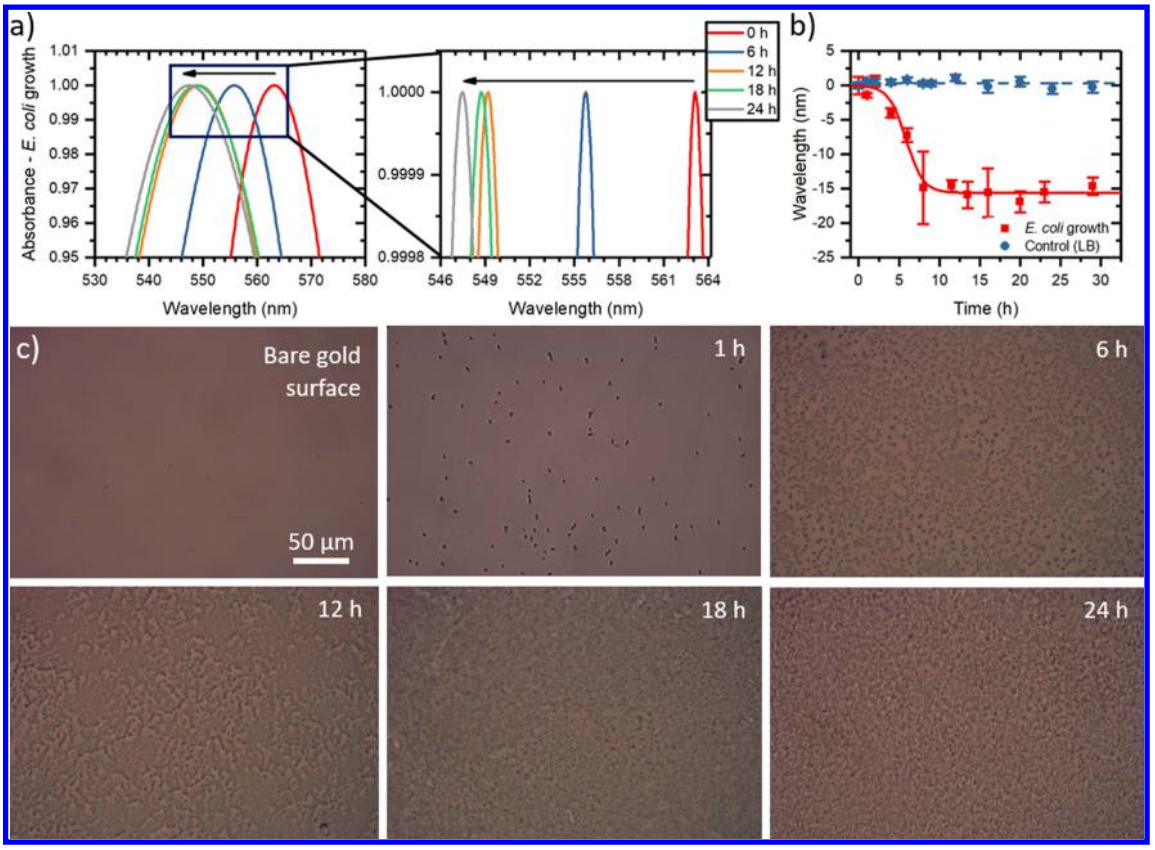

Figure 2. Noncontinuous LSPR monitoring the bacterial adhesion and biofilm formation in the LB culture media. While the bacterial growth is performed at 37 °C in an incubator, the absorbance data are obtained at room temperature and take less than 10 s for each measurement. (a) Normalized absorbance spectra for the LSPR biochip incubated with an *E. coli* sample in the LB medium, with zoomed-in details in the wavelength of 546−564 nm region. The peak position shifts to shorter wavelengths during biofilm assembly. The black arrow highlights the progressive blue shift due to microbial biofilm assembly. (b) Absorbance peak position as a function of time. The control experiment performed using only LB culture media produces a negligible shift in the signal (blue circles) when compared with the sample containing *E. coli* (red squares). Each data point corresponds to at least 3 repetitive experiments ($n \geq 3$), with the error bars denoting the standard error of mean (SE). (c) Bacterial growth monitored at 0, 1, 6, 12, 18, and 24 h, captured by bright-field microscopy (Eclipse Ti−U, Nikon Instruments Inc.). The series of images illustrate the progress of the biofilm formation in a LSPR biochip.

SiO_2 substrate is optically translucent and pink in color due to the presence of plasmonic Au nanostructures. The Au nanostructures have a characteristic pillar shape, with the schematic shown in Figure 1b. The morphological features of the substrate such as the size of the Au NM, gap size between NMs, and their surface density is characterized by using tapping mode atomic force microscopy (AFM) and scanning electron microscopy (SEM), which provide detailed nanometric features of the LSPR substrate (Figure 1). Based on the AFM images (Figure 1c and d), the Au NMs are quasi-uniformly distributed on the SiO_2 surface ($\sim 10^6-10^8$ NM cm^{-2}) with a root-mean-square roughness of 2.0 ± 0.1 nm. Based on the high contrast images between Au NMs and the glass substrate obtained by SEM (Figure 1e and f), the average diameter of NMs is 29 ± 0.3 nm (standard error of mean, SE) and 29 ± 14 nm (standard deviation, SD). The average spacing among the Au NMs is 9 ± 1 nm (SE) and 9 ± 6 nm (SD).

For LSPR sensing applications, the average refractive index (RI) sensitivity of our NM LSPR substrate is estimated as 98.6 nm RIU^{-1} (see more details in the Supporting Information). The sensitivity of the Au NM can be tuned by changing the size and gaps of the NM structures (discussed in our previous work[40]). Note that the size and morphology of Au nanostructures are also crucial for the biocompatibility of the LSPR substrate when it is in direct contact with live entities such as bacteria, virus, and eukaryotic cells.[40] In later sections we will discuss the effects of the continuous exposure of LSPR illumination on the bacterial growth.

LSPR Monitoring of Bacteria Biofilm Formation. The local sensitivity and the reliability of our Au NM LSPR substrate have been exploited to develop a new characterization tool to monitor the *E. coli* growth and biofilm formation. *E. coli* strains can be both nonpathogenic and pathogenic. The nonpathogenic ones are harmless and easy to manipulate, and hence will be used as our model microorganism to optimize the sensing procedure. However, the pathogenic *E. coli* strains are important since they are responsible for a wide range of diseases, e.g., urogenital infections where bacterial cells form biofilms.[44] Nevertheless, our studies can be easily expanded to other bacterial systems. Below we will illustrate both noncontinuous and real-time LSPR monitoring of bacterial biofilm formation by using a model nonpathogenic *E. coli* system.

Noncontinuous Monitoring. To study the biofilm formation, an inoculum of *E. coli* (125 µL, 2×10^7 CFU mL^{-1}) is loaded into our LSPR biochip and the bacterial growth is then monitored for about 30 h. For the noncontinuous monitoring, the LSPR biochip is removed from an incubator at 37 °C only periodically when it is required to collect the absorbance spectrum (~10 s).

DOI: 10.1021/acssensors.8b00287
ACS Sens. 2018, 3, 1499−1509

As shown in Figure 2a and b, bacterial growth and adhesion on the Au NM substrate produce a significant blue shift in the absorbance peak of the Au NM, which can be attributed to the charge changes in the overall system upon biofilm formation. As the bacterial film assembly progresses, the charge on the NM substrate increases with the increasing amount of bacteria, protein, and polysaccharide secretion,[45,46] which eventually leads to the formation of biofilm. Recall that biofilm is a slimy matrix composed of mostly proteins and polysaccharides, the latter being negatively charged at physiological pH.[47] The increase in the surface charge of Au NM during the biofilm formation further leads to an enhanced frequency of plasmonic resonances because the frequency of plasmons is directly proportional to the amount of the charge on the plasmonic material. The increase in the frequency also causes a decrease in the LSPR wavelength, suggesting that the observed blue shifts in the wavelength peak correspond to the bacterial biofilm formation. Red square symbols in Figure 2b illustrate that the LSPR signal saturates around 8 h, correlated with the completion of the biofilm assembly. For comparison, by incubating the LSPR substrate with the culture medium (LB) for 30 h, only negligible wavelength shift is observed (blue circles in Figure 2b).

The LSPR resonance wavelength versus time data (Figure 2b, red squares) is fitted by using a modified logistic-type function:

$$\Delta\lambda = b + \frac{a - b}{1 + e^{k(t-t^*)}}, \quad (1)$$

where $\Delta\lambda$ is the wavelength shift in nanometer, a and b are the initial and the final wavelength values, respectively, k is a rate parameter, and t^* corresponds to the time upon which the growth and biofilm formation rates are maximized and half of the wavelength shift $(a-b)$ is achieved. By fixing the initial value ($a = 0$), the best fit of the experimental responses due to the bacterial growth yields $b=-15.6 \pm 0.5$ nm, $k = 0.93 \pm 0.18$ h^{-1}, and $t^*=5.8 \pm 0.3$ h.

The biofilm formation is also confirmed by bright-field microscopy (Figure 2c), which reveals that bacterial growth is barely affected by the nature of the plasmonic substrate nor the LSPR sensing setup. This observation is promising since LSPR substrate has been reported to induce local temperature jump and cause cell death.[48] Our results demonstrate that our Au NM LSPR substrate is biocompatible and enables the bacteria to form biofilm with sustained viability for more than 30 h. This simple LSPR platform also allows us to easily evaluate detailed kinetics underlying the biofilm formation and can be used to compare different types of microorganisms or testing the effect of drugs on the bacterial growth.

However, to obtain each measurement point at a specific time (shown in Figure 2b), the LSPR biochip has to be removed from the 37 °C incubator periodically to capture LSPR signals; hence, some inevitable changes in the LSPR biochip position through the manual alignment and the environmental light have led to some random fluctuations in the resonance peak wavelength (the error bars in Figure 2b represent the standard error of mean, $n \geq 3$). To reduce the contribution of these random fluctuations, we present the real-time continuous monitoring procedure below.

Real-Time Continuous Monitoring. To enhance the sampling frequency and overcome the noise issues from the noncontinuous monitoring, we have developed an automatized system to provide the real-time monitoring of the local refractive index changes (hence the LSPR signals) as soon as the *E. coli* is deposited in the PDMS well of the LSPR biochip. To prevent sample evaporation, the LSPR biochip is confined in a transparent chamber with a water reservoir. Both bacterial growth and the absorbance spectrum are recorded in a Faraday cage to eliminate the noise caused by the environmental light. Once the chip is orthogonally aligned between the two optical fibers, we use a custom-made software to record the absorbance spectrum every minute for a duration of 24 h, thus achieving a much better resolution than those from the noncontinuous measurements. Sensor signals obtained during the first 24 h when an LSPR chip is incubated with an *E. coli* sample in the LB medium, are shown in the Supporting Information, consistent with the noncontinuous measurements.

The stability of the LSPR reading and any nonspecific response resulting from the continuous illumination of the LSPR biochip is first evaluated by recording the transmitted light of a bare Au NM LSPR sensor, in contact with air, for 24 h. The LSPR signals appear to be quite stable for the whole duration of the experiment (purple triangles in Figure 3a). Thereafter, the same real-time monitoring LSPR procedure is used to compare responses from different samples: plain

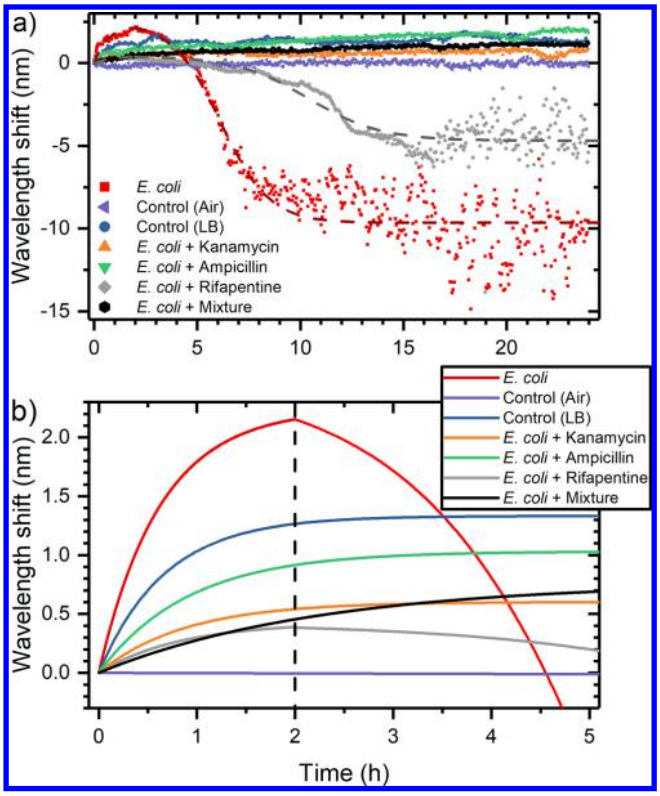

Figure 3. Real-time monitoring of bacterial adhesion and biofilm formation. (a) Resonance wavelength as a function of time for the control (LB), *E. coli*, and *E. coli* growing in the presence of various antibiotics and antibiotic mixture (kanamycin: 100 μg mL^{-1}, ampicillin: 100 μg mL^{-1}, rifapentine: 1 μg mL^{-1}). The stability of the sensing platform is evaluated by measuring the resonance peak of the LSPR biochip for 24 h when exposed to air (purple triangles). Peak positions are estimated by fitting the spectra in the 520–600 nm region using a spline function. (b) Magnification of the sensor responses for the first 5 h where the experimental data are shown with the best curve fits.

DOI: 10.1021/acssensors.8b00287
ACS Sens. 2018, 3, 1499–1509

Table 2. Parameters Resulting from the Best Fit of the Absorption Maximum Position Data Shown in Figure 3, from the Real-Time Monitoring[a]

	exponential model		logistic-type model			
sample	A (nm)	B (h)	a (nm)	b (nm)	k (h^{-1})	t^* (h)
E. coli	2.24 ± 0.02	1.60 ± 0.09	2.5 ± 0.05	−9.64 ± 0.08	0.85 ± 0.03	6.14 ± 0.04
Control (LB)	1.33 ± 0.01	1.49 ± 0.07				
E. coli+Kanamycin	0.60 ± 0.01	1.14 ± 0.09				
E. coli+Ampicillin	1.03 ± 0.01	1.09 ± 0.05				
E. coli+Rifapentine	0.43 ± 0.01	1.20 ± 0.10	0.43 ± 0.01	−4.69 ± 0.06	0.57 ± 0.03	10.40 ± 0.10
E. coli+Mixture	0.77 ± 0.02	0.44 ± 0.03				

[a]The naked LSPR substrate (control (Air)) shows negligible wavelength shift, hence data not included in this table.

culture medium (LB), *E. coli* in LB medium, and *E. coli* treated with different antibiotics (kanamycin at 100 μg mL^{-1}, ampicillin at 100 μg mL^{-1}, rifapentine at 1 μg mL^{-1}, and a mixture of the three drugs (kanamycin at 100 μg mL^{-1}; ampicillin at 100 μg mL^{-1}; rifapentine at 1 μg mL^{-1})). These antimicrobial agents attack different aspects of bacteria metabolisms. Kanamycin and ampicillin are standard antibiotics: kanamycin interacts with the ribosomes affecting protein synthesis while ampicillin inhibits the transpeptidase, an enzyme involved in cell wall assembling. On the other hand, rifapentine affects the RNA polymerase and has been shown to inhibit curli-dependent biofilm formation without killing the bacteria at a concentration of a few μg mL^{-1}.[49]

Biofilm growth is controlled by a variety of physical, chemical, and biological phenomena, resulting in cell-to-substrate adhesion and cell-to-cell cohesion events.[19] Different from the noncontinuous measurements (data only captured every 1−2 h), a slight red shift in the wavelength is observed during the first 2 h of the real-time monitoring experiments (see Figure 3). The LSPR substrate is first modified by an initial conditioning layer, which promotes the bacteria anchorage and irreversible adhesion. The observed red shift is likely due to the increase in the local dielectric constant of the Au NM structures from the bacterial and protein adhesion on the Au NM substrates since LSPR signal is sensitive to the variation in the local dielectric constant of the sample volume, which extends by ∼30 nm from the top of the Au NM surface.[50] After 2 h, the Au NM LSPR substrate is completely covered with either bacteria or conditioning biomolecules, preventing further shifts in the local dielectric constant, and thus the LSPR signal starts to exhibit blue shifts. This change of regime is evident in Figure 3b (see the vertical dashed line), where the sensor response from *E. coli* in LB without any antibiotics (red curve) displays a clear peak and a slope change at about 2 h.

Figure 3a also shows some scattering in the LSPR signal for *E. coli* and *E. coli* treated with rifapentine. They are likely due to the high turbidity of the sample, caused by large number of cells in the LSPR-PDMS wells, which makes it difficult to clearly identify the resonance peak. However, this effect does not alter the overall wavelength shift in the resonance peak.

The recorded absorbance spectra captured every minute for all experiments are fitted using a spline function, providing the resonance wavelength shift data shown in Figure 3a. The experimental results show that biofilms treated with conventional antibiotics (kanamycin (orange symbols) and ampicillin (green symbols)) lead to signals similar to the one obtained by the control experiment (LB in blue symbols); see Figure 3. On the other hand, rifapentine (gray symbols) at an effective concentration of 1 μg mL^{-1}[49] prevents the cell adhesion but does not eradicate the bacteria, resulting in a smaller wavelength shift than the one obtained by nontreated *E. coli* (red symbols).

Interestingly, the response of the *E. coli* treated by the mixed drug system is similar to the one treated with rifapentine during the first 2 h, with the black and the gray curves almost overlapping (see Figure 3b). However, after 2 h, the resonance peak from the mixed drug system shifts to a larger wavelength, reaching similar saturation values as those of the *E. coli* treated with ampicillin and kanamycin.

The wavelength shifts from all these cases are fitted by an exponential model:

$$\Delta\lambda = A(1 + e^{-Bt}), \quad (2)$$

where A and B are the amplitude of the exponential and a rate parameter, respectively.

The comparison of the fitted responses of the tested samples is shown in Figure 3b. Table 2 shows values of fitted parameters based on the best fit of the experimental data using the exponential (eq 2) or/and the logistic (eq 1) type models. The rate parameters k and t^*, the time at which the biofilm formation rate is maximized, can be correlated with the dampening effect on the biofilm formation due to an adhesion inhibiting drug like rifapentine. When rifapentine is added to the culture medium, surface coating rate (k) is significantly reduced (0.85 ± 0.03 h^{-1} versus 0.57 ± 0.03 h^{-1} for *E. coli* and *E. coli* treated with rifapentine, respectively), while the time t^* to achieve half of the wavelength shift ($b-a$) increases (6.14 ± 0.04 h versus 10.39 ± 0.11 h, respectively). These results can be very valuable for drug screening studies, since the LSPR signals can be utilized to identify new molecules, which can be combined with conventional antibiotics to either prevent the formation of the microbial superstructure or attack the existing biofilm.

Figure 4 provides a general summary of the biofilm LSPR responses under different experimental conditions (noncontinuous versus real-time), showing wavelength shifts at 24 h. Note both *E. coli* - Noncontinuous and *E. coli* - Real-time tests shown are performed without any drugs or chemicals. In the noncontinuous case, the LSPR biochip is mostly kept in an incubator at 37 °C for the entire experiment, while in the real-time experiment, the biochip is illuminated with a white light for 24 h, which results in a slightly smaller wavelength shift (−11.8 ± 3.4 nm), compared to the noncontinuous test (−14.8 ± 1.3 nm). Among the real-time experiments, the control sample (LB), *E. coli* treated with kanamycin, ampicillin, and the antibiotic mixture exhibit similar results in the wavelength shift. This is due to the antimicrobial properties of the two conventional drugs which kill mostly all the bacteria

DOI: 10.1021/acssensors.8b00287
ACS Sens. 2018, 3, 1499−1509

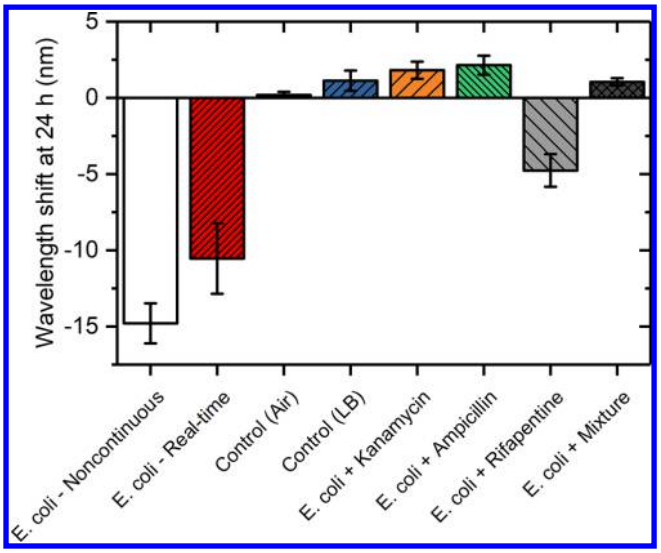

Figure 4. Comparison at 24 h between nontreated *E. coli*, culture media LB, and bacteria under different antibiotic treatments. Real-time measurements (*E. coli* - Real-time) require the continuous illumination of the sample with a white light, inducing additional stress on bacteria than noncontinuous measurements (*E. coli* - Noncontinuous), which results in a slightly smaller wavelength shift (-14.8 ± 1.3 nm and -11.8 ± 3.4 nm for *E. coli* - Noncontinuous and *E. coli* - Real-time, respectively). While LB, *E. coli* treated with kanamycin, and ampicillin are mostly comparable, the rifapentine-treated sample produces a signal of -4.8 ± 1.1 nm, which is about 50% of the one due to nontreated cells. *Note: The error bars represent standard error of the mean. Each error bar corresponds to at least 3 sets of experiments* ($n \geq 3$).

before they are able to adhere onto the sensor surface and form the biofilm. On the other hand, the LSPR biochip incubated with rifapentine-treated *E. coli* produces a wavelength shift of -4.8 ± 1.1 nm, which is about 50% of those with nontreated bacteria cells. These results are consistent with the intended drug mechanisms of the three antibiotics used: antimicrobial activity versus bacterial adhesion prevention. Indeed, using a drug (like refapentine) to attack biofilm formation is not sufficient to fight the bacterial infection. As evidenced by the response of the LSPR biochip of *E. coli* treated with a mixture of antibiotics (*E. coli* + Mixture series of data in Figure 3 and Figure 4), a more effective strategy to fight bacterial biofilm is to combine conventional bacterial killing antibiotics with drugs that target specifically to the biofilm structure.

Since the wavelength shift in the adsorption peaks at 24 h is related to the amount of bacterial cells and EPS absorbed onto the LSPR substrate, these LSPR signals can be compared with the standard end-point microbiology assays such as crystal violet staining assay for the biofilm mass evaluation, see section below (see protocol details in Experimental Section).

LSPR Sensor Response versus Crystal Violet Staining and Viability Test. In order to validate the results of our LSPR-based methodology, two independent standard staining procedures have been used to compare the mass and cell viability of bacterial biofilms. Crystal violet (CV) assay is the most common methodology to evaluate biofilm formation and is based on the direct measurement of microbial biomass. This technique is commonly performed by comparing the absorbance at 570 nm of different samples after 24 h bacterial growth with CV staining, in a 96-well plate. Since this is a disruptive assay, CV staining does not allow investigations of dynamic phenomena. After subtracting the contribution of the culture media (LB), the absorbance intensities at 570 nm for stained samples of *E. coli* treated with kanamycin, ampicillin, and rifapentine are normalized with respect to the intensity value of nontreated *E. coli*, which is considered as 100% of the response of the assay. In Figure 5a, the results provided by CV staining (blue bars) are compared with the wavelength shifts (normalized by the 24 h value) captured by our LSPR biochip (red bars).

Consistent with the results illustrated by our LSPR-based biosensor, the treatment with kanamycin and ampicillin provides minor signals since most of the bacteria are killed by these two antibiotics. On the other hand, the treatment with rifapentine is less aggressive since it affects only the adhesion properties of the microbes. This produces an absorbance value at 570 nm, which is about 50% of the value from the nontreated *E. coli*, thus being in excellent agreement with the measurements provided by our LSPR based biochip.

As previously reported, the oscillation of the electrons related to the LSPR sensing can lead to local temperature increase, which can kill bacterial cells.[48] As a precaution, we next evaluate how our LSPR based detection system affects the cell vitality. For this reason we use the LIVE/DEAD Baclight Bacterial Viability Kit, which allows us to discriminate between dead (red dye) and living (green dye) cells by fluorescence microscopy. This test has been performed directly on the LSPR Au NM substrate after 24 h of bacterial growth; see images shown in Figure 5b (I, II, III).

The portion of living cells on a glass slide (Figure 5b panel I), being used as a control study, yields about 95%. For a non-illuminated LSPR substrate (Figure 5b panel II), this value is about 85%. On the other hand, the survival percentage of the bacteria reduces to 65% on the LSPR biochip used for real-time measurements (Figure 5b panel III), likely due to the local stress induced by the continuous light irradiation. This decrease in vitality for continuously illuminated sample matches the difference observed in the LSPR response between the noncontinuous and real-time LSPR measurements (in Figure 4). Nevertheless, despite the substrate and stress influence on the bacterial cell vitality, the bacterial cells are still able to multiply and adhere onto the substrate with biofilm formation. For future research, we plan to include a shutter to illuminate the LSPR biochip only briefly (few seconds) to collect the transmitted light. This will reduce the stress applied to the microbial cells, thus improving their vitality.

CONCLUSIONS

We report the application of an LSPR-based sensor for the direct, real-time, and nondisruptive label-free characterization of bacterial biofilm in a liquid environment. Our LSPR sensor platform is able to capture the biofilm assembling kinetics and illustrate how such process is affected by different antibiotics. The sensing device is based on Au nanoplasmonic structures realized by a cost-effective nanofabrication process. The quantification of *E. coli* biofilm formation by our LSPR-based device shows excellent agreement with the measurements performed by conventional microbiology techniques (e.g., crystal violet assay and viability staining), thus proving the reliability and the robustness of our approach and paving the way to its utility as a promising tool for characterizing bacterial biofilms. Moreover, we demonstrate how efficacy of drugs can be tested using our LSPR biochips, which lays the foundation to apply LSPR technology in antibiotic drug discovery. Our

DOI: 10.1021/acssensors.8b00287
ACS Sens. 2018, 3, 1499−1509

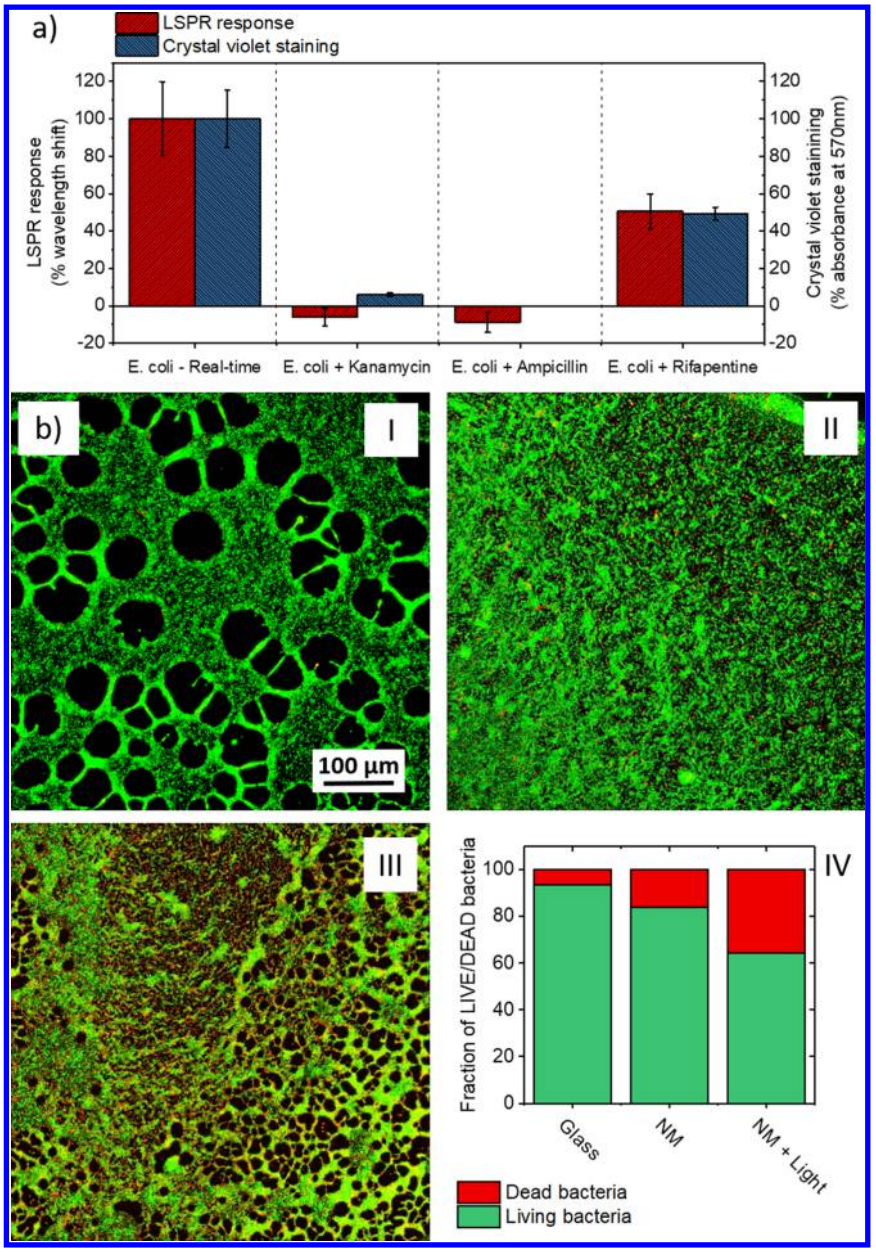

Figure 5. (a) Biofilm biomass estimation using CV staining (blue bars) and normalized LSPR sensor responses for various samples (red bars) where the output of nontreated *E. coli* represents 100% of the response. The errors bars represent SE. Each error bar corresponds to at least three sets of experiments. (b) LIVE/DEAD BacLight Bacterial Viability staining to estimate the effect of the nanoplasmonic structures on cells viability. The experiment is performed using two different fluorescent dyes (SYTO 9 and propidium iodide), emitting in the green and red spectral regions, being specific for living and dead cells, respectively. Fluorescence images of bacteria growing on glass (I), on LSPR Au NM substrate without light exposure (II), and on the LSPR biochip at the end of the 24 h real-time measurement (III). (IV) Fractions of living and dead cells in (I), (II), and (III) images.

detection methodology can be easily used on other bacteria systems and can also be adapted to study mixed-species biofilm formation. In addition, our real-time setup is extremely flexible since it can be easily integrated with a temperature control system and can acquire data for several days without any action from the operator. One potential future application of our LSPR system is miniaturized portable version, which can be valuable for in situ monitoring of biofilm formation in sensitive areas such as hospitals or food industries where bacterial contamination is a looming concern.

■ ASSOCIATED CONTENT

Supporting Information

The Supporting Information is available free of charge on the ACS Publications website at DOI: 10.1021/acssensors.8b00287.

Detection and interrogation techniques of microbial biofilms, Size characterization of Gold nanomushrooms, Sensitivity characterization of the LSPR biochip, Wavelength shift due to microbial biofilm formation on an LSPR substrate, Crystal violet staining protocol, Viability staining protocol. (PDF)

DOI: 10.1021/acssensors.8b00287
ACS Sens. 2018, 3, 1499−1509

AUTHOR INFORMATION

Corresponding Authors

*E-mail: riccardo.funari@oist.jp.

*E-mail: amy.shen@oist.jp.

ORCID

Amy Q. Shen: 0000-0002-1222-6264

Author Contributions

¶Riccardo Funari and Nikhil Bhalla contributed equally.

Notes

The authors declare no competing financial interest.

ACKNOWLEDGMENTS

We gratefully acknowledge the support of the Okinawa Institute of Science and Technology Graduate University (OIST) with subsidy funding from the Cabinet Office, Government of Japan. A.Q.S. also acknowledges funding from the Japan Society for the Promotion of Science (Grants-in-Aid for Scientific Research (C), Grant No. 17K06173).

REFERENCES

(1) Flemming, H.-C.; Wingender, J.; Szewzyk, U.; Steinberg, P.; Rice, S. A.; Kjelleberg, S. Biofilms: an emergent form of bacterial life. *Nat. Rev. Microbiol.* **2016**, *14*, 563−575.

(2) Donlan, R. M. Biofilms: microbial life on surfaces. *Emerging Infect. Dis.* **2002**, *8*, 881−890.

(3) Flemming, H.-C.; Neu, T. R.; Wozniak, D. J. The EPS matrix: the "house of biofilm cells". *Journal of bacteriology* **2007**, *189*, 7945−7947.

(4) Davies, D. Understanding biofilm resistance to antibacterial agents. *Nat. Rev. Drug Discovery* **2003**, *2*, 114−122.

(5) Stewart, P. S.; Costerton, J. W. Antibiotic resistance of bacteria in biofilms. *Lancet* **2001**, *358*, 135−138.

(6) Stewart, P. S. Mechanisms of antibiotic resistance in bacterial biofilms. *Int. J. Med. Microbiol.* **2002**, *292*, 107−113.

(7) Høiby, N.; Bjarnsholt, T.; Givskov, M.; Molin, S.; Ciofu, O. Antibiotic resistance of bacterial biofilms. *Int. J. Antimicrob. Agents* **2010**, *35*, 322−332.

(8) Halan, B.; Buehler, K.; Schmid, A. Biofilms as living catalysts in continuous chemical syntheses. *Trends Biotechnol.* **2012**, *30*, 453−465.

(9) Kostakioti, M.; Hadjifrangiskou, M.; Hultgren, S. J. Bacterial biofilms: development, dispersal, and therapeutic strategies in the dawn of the postantibiotic era. *Cold Spring Harbor Perspect. Med.* **2013**, *3*, a010306.

(10) Wingender, J.; Flemming, H.-C. Biofilms in drinking water and their role as reservoir for pathogens. *Int. J. Hyg. Environ. Health* **2011**, *214*, 417−423.

(11) World Health Organization *Global antimicrobial resistance surveillance system (GLASS) report - Early implementation 2016−2017*; World Health Organization, 2017.

(12) Jo, N.; Kim, B.; Lee, S.-M.; Oh, J.; Park, I. H.; Lim, K. J.; Shin, J.-S.; Yoo, K.-H. Aptamer-functionalized capacitance sensors for real-time monitoring of bacterial growth and antibiotic susceptibility. *Biosens. Bioelectron.* **2018**, *102*, 164−170.

(13) Brosel-Oliu, S.; Ferreira, R.; Uria, N.; Abramova, N.; Gargallo, R.; Muñoz-Pascual, F.-X.; Bratov, A. Novel impedimetric aptasensor for label-free detection of Escherichia coli O157: H7. *Sens. Actuators, B* **2018**, *255*, 2988−2995.

(14) Olivares, E.; Badel-Berchoux, S.; Provot, C.; Jaulhac, B.; Prévost, G.; Bernardi, T.; Jehl, F. The BioFilm Ring Test: a rapid method for routine analysis of Pseudomonas aeruginosa biofilm formation kinetics. *J. Clin. Microbiol.* **2016**, *54*, 657−661.

(15) Peeters, E.; Nelis, H. J.; Coenye, T. Comparison of multiple methods for quantification of microbial biofilms grown in microtiter plates. *J. Microbiol. Methods* **2008**, *72*, 157−165.

(16) Stepanović, S.; Vuković, D.; Hola, V.; Di Bonaventura, G.; Djukić, S.; Ćirković, I.; Ruzicka, F. Quantification of biofilm in microtiter plates: overview of testing conditions and practical recommendations for assessment of biofilm production by staphylococci. *Apmis* **2007**, *115*, 891−899.

(17) Hoffman, L. R.; D'argenio, D. A.; MacCoss, M. J.; Zhang, Z.; Jones, R. A.; Miller, S. I. Aminoglycoside antibiotics induce bacterial biofilm formation. *Nature* **2005**, *436*, 1171.

(18) Goeres, D. M.; Hamilton, M. A.; Beck, N. A.; Buckingham-Meyer, K.; Hilyard, J. D.; Loetterle, L. R.; Lorenz, L. A.; Walker, D. K.; Stewart, P. S. A method for growing a biofilm under low shear at the air−liquid interface using the drip flow biofilm reactor. *Nat. Protoc.* **2009**, *4*, 783−788.

(19) Garrett, T. R.; Bhakoo, M.; Zhang, Z. Bacterial adhesion and biofilms on surfaces. *Prog. Nat. Sci.* **2008**, *18*, 1049−1056.

(20) Bremer, P. J.; Geese, G. G.; Drake, B. Atomic force microscopy examination of the topography of a hydrated bacterial biofilm on a copper surface. *Curr. Microbiol.* **1992**, *24*, 223−230.

(21) Ansari, M. J.; Al-Ghamdi, A.; Usmani, S.; Al-Waili, N. S.; Sharma, D.; Nuru, A.; Al-Attal, Y. Effect of jujube honey on Candida albicans growth and biofilm formation. *Arch. Med. Res.* **2013**, *44*, 352−360.

(22) Potthoff, E.; Ossola, D.; Zambelli, T.; Vorholt, J. A. Bacterial adhesion force quantification by fluidic force microscopy. *Nanoscale* **2015**, *7*, 4070−4079.

(23) Huang, Q.; Wu, H.; Cai, P.; Fein, J. B.; Chen, W. Atomic force microscopy measurements of bacterial adhesion and biofilm formation onto clay-sized particles. *Sci. Rep.* **2015**, *5*, 16857.

(24) Schofield, A. L.; Rudd, T. R.; Martin, D. S.; Fernig, D. G.; Edwards, C. Real-time monitoring of the development and stability of biofilms of Streptococcus mutans using the quartz crystal microbalance with dissipation monitoring. *Biosens. Bioelectron.* **2007**, *23*, 407−413.

(25) Gutiérrez, D.; Hidalgo-Cantabrana, C.; Rodríguez, A.; García, P.; Ruas-Madiedo, P. Monitoring in real time the formation and removal of biofilms from clinical related pathogens using an impedance-based technology. *PLoS One* **2016**, *11*, e0163966.

(26) Pires, L.; Sachsenheimer, K.; Kleintschek, T.; Waldbaur, A.; Schwartz, T.; Rapp, B. E. Online monitoring of biofilm growth and activity using a combined multi-channel impedimetric and amperometric sensor. *Biosens. Bioelectron.* **2013**, *47*, 157−163.

(27) Goikoetxea, E.; Routkevitch, D.; De Weerdt, A.; Green, J. J.; Steenackers, H.; Braeken, D. Impedimetric fingerprinting and structural analysis of isogenic E. coli biofilms using multielectrode arrays. *Sens. Actuators, B* **2018**, *263*, 319−326.

(28) Matsuura, K.; Asano, Y.; Yamada, A.; Naruse, K. Detection of Micrococcus Luteus biofilm formation in microfluidic environments by pH measurement using an ion-sensitive field-effect transistor. *Sensors* **2013**, *13*, 2484−2493.

(29) Filion-Côté, S.; Melaine, F.; Kirk, A. G.; Tabrizian, M. Monitoring of bacterial film formation and its breakdown with an angular-based surface plasmon resonance biosensor. *Analyst* **2017**, *142*, 2386−2394.

(30) Suzuki, N.; Yoshida, A.; Nakano, Y. Quantitative analysis of multi-species oral biofilms by TaqMan Real-Time PCR. *Clin. Med. Res.* **2005**, *3*, 176−185.

(31) Donlan, R.; Piede, J.; Heyes, C.; Sanii, L.; Murga, R.; Edmonds, P.; El-Sayed, I.; El-Sayed, M. Model system for growing and quantifying Streptococcus pneumoniae biofilms in situ and in real time. *Applied and environmental microbiology* **2004**, *70*, 4980−4988.

(32) Bruchmann, J.; Sachsenheimer, K.; Rapp, B. E.; Schwartz, T. Multi-channel microfluidic biosensor platform applied for online monitoring and screening of biofilm formation and activity. *PLoS One* **2015**, *10*, e0117300.

(33) Anker, J. N.; Hall, W. P.; Lyandres, O.; Shah, N. C.; Zhao, J.; Van Duyne, R. P. Biosensing with plasmonic nanosensors. *Nat. Mater.* **2008**, *7*, 442−453.

DOI: 10.1021/acssensors.8b00287
ACS Sens. 2018, 3, 1499−1509

(34) Špačková, B.; Wrobel, P.; Bocková, M.; Homola, J. Optical biosensors based on plasmonic nanostructures: a review. *Proc. IEEE* **2016**, *104*, 2380−2408.
(35) Willets, K. A.; Van Duyne, R. P. Localized surface plasmon resonance spectroscopy and sensing. *Annu. Rev. Phys. Chem.* **2007**, *58*, 267−297.
(36) Hammond, J. L.; Bhalla, N.; Rafiee, S. D.; Estrela, P. Localized surface plasmon resonance as a biosensing platform for developing countries. *Biosensors* **2014**, *4*, 172−188.
(37) Meeker, D. G.; Jenkins, S. V.; Miller, E. K.; Beenken, K. E.; Loughran, A. J.; Powless, A.; Muldoon, T. J.; Galanzha, E. I.; Zharov, V. P.; Smeltzer, M. S.; Chen, J. Synergistic photothermal and antibiotic killing of biofilm-associated Staphylococcus aureus using targeted antibiotic-loaded gold nanoconstructs. *ACS Infect. Dis.* **2016**, *2*, 241−250.
(38) Ding, X.; Yuan, P.; Gao, N.; Zhu, H.; Yang, Y. Y.; Xu, Q.-H. Au-Ag core-shell nanoparticles for simultaneous bacterial imaging and synergistic antibacterial activity. *Nanomedicine* **2017**, *13*, 297−305.
(39) Pallavicini, P.; Dona, A.; Taglietti, A.; Minzioni, P.; Patrini, M.; Dacarro, G.; Chirico, G.; Sironi, L.; Bloise, N.; Visai, L.; Scarabelli, L. Self-assembled monolayers of gold nanostars: a convenient tool for near-IR photothermal biofilm eradication. *Chem. Commun.* **2014**, *50*, 1969−1971.
(40) Bhalla, N.; Sathish, S.; Sinha, A.; Shen, A. Q. Large-Scale Nanophotonic Structures for Long-Term Monitoring of Cell Proliferation. *Advanced Biosystems* **2018**, *2*, 1700258.
(41) Bhalla, N.; Sathish, S.; Galvin, C. J.; Campbell, R. A.; Sinha, A.; Shen, A. Q. Plasma assisted large-scale nanoassembly of metal-insulator bioplasmonic mushrooms. *ACS Appl. Mater. Interfaces* **2018**, *10*, 219−226.
(42) O'Toole, G. A. Microtiter dish biofilm formation assay. *J. Visualized Exp.* **2011**, No. e2437, DOI: 10.3791/2437.
(43) Feoktistova, M.; Geserick, P.; Leverkus, M. Crystal violet assay for determining viability of cultured cells. *Cold Spring Harbor Protocols* **2016**, *2016*, pdb.prot087379.
(44) Kaper, J. B.; Nataro, J. P.; Mobley, H. L. Pathogenic escherichia coli. *Nat. Rev. Microbiol.* **2004**, *2*, 123.
(45) Kang, F.; Alvarez, P. J.; Zhu, D. Microbial extracellular polymeric substances reduce Ag^{+} to silver nanoparticles and antagonize bactericidal activity. *Environ. Sci. Technol.* **2014**, *48*, 316−322.
(46) Kroll, A.; Behra, R.; Kaegi, R.; Sigg, L. Extracellular polymeric substances (EPS) of freshwater biofilms stabilize and modify CeO2 and Ag nanoparticles. *PLoS One* **2014**, *9*, e110709.
(47) Wingender, J.; Neu, T. R.; Flemming, H.-C. *Microbial extracellular polymeric substances*; Springer, 1999; pp 1−19.
(48) Pihl, M.; Bruzell, E.; Andersson, M. Bacterial biofilm elimination using gold nanorod localised surface plasmon resonance generated heat. *Mater. Sci. Eng., C* **2017**, *80*, 54−58.
(49) Maher, M. C.; Lim, J. Y.; Gunawan, C.; Cegelski, L. Cell-based high-throughput screening identifies rifapentine as an inhibitor of amyloid and biofilm formation in Escherichia coli. *ACS Infect. Dis.* **2015**, *1*, 460−468.
(50) Zalyubovskiy, S. J.; Bogdanova, M.; Deinega, A.; Lozovik, Y.; Pris, A. D.; An, K. H.; Hall, W. P.; Potyrailo, R. A. Theoretical limit of localized surface plasmon resonance sensitivity to local refractive index change and its comparison to conventional surface plasmon resonance sensor. *J. Opt. Soc. Am. A* **2012**, *29*, 994−1002.

DOI: 10.1021/acssensors.8b00287
ACS Sens. 2018, 3, 1499−1509